NANO LETTERS

Letter

pubs.acs.org/NanoLett

Engineering Ultra-Low Work Function of Graphene

Hongyuan Yuan,[*,†] Shuai Chang,[‡] Igor Bargatin,[#] Ning C. Wang,[‡] Daniel C. Riley,[†] Haotian Wang,[∥] Jared W. Schwede,[†] J. Provine,[‡] Eric Pop,[‡] Zhi-Xun Shen,[†,∥] Piero A. Pianetta,[‡,⊥] Nicholas A. Melosh,[§] and Roger T. Howe[‡]

[†]Department of Physics, [‡]Department of Electrical Engineering, [§]Department of Material Science and Engineering, and [∥]Department of Applied Physics, Stanford University, Stanford, California 94305, United States

[⊥]Stanford Synchrotron Radiation Lightsource, SLAC National Accelerator Laboratory, 2575 Sand Hill Road, MS31, Menlo Park, California 94205, United States

[#]Department of Mechanical Engineering and Applied Mechanics, University of Pennsylvania, Philadelphia, Pennsylvania 19104, United States

S *Supporting Information*

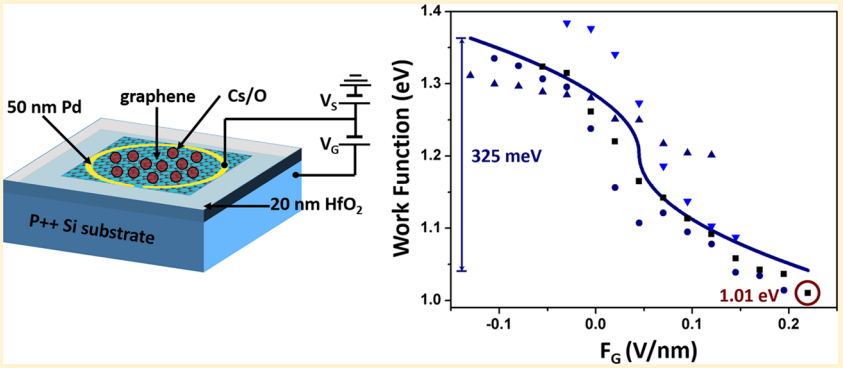

ABSTRACT: Low work function materials are critical for energy conversion and electron emission applications. Here, we demonstrate for the first time that an ultralow work function graphene is achieved by combining electrostatic gating with a Cs/O surface coating. A simple device is built from large-area monolayer graphene grown by chemical vapor deposition, transferred onto 20 nm HfO_2 on Si, enabling high electric fields capacitive charge accumulation in the graphene. We first observed over 0.7 eV work function change due to electrostatic gating as measured by scanning Kelvin probe force microscopy and confirmed by conductivity measurements. The deposition of Cs/O further reduced the work function, as measured by photoemission in an ultrahigh vacuum environment, which reaches nearly 1 eV, the lowest reported to date for a conductive, nondiamond material.

KEYWORDS: *Graphene, work function, electrostatic gating, transistor, photoemission, scanning Kelvin probe force microscopy*

The work function (Φ) of a material is the energy difference between its vacuum level and Fermi level (E_F). It is not a fundamental constant but can be tuned through doping or surface engineering. Materials with very low work function can significantly improve many electronic device technologies including organic electronics[1−4] and electron emission devices.[5−11] Similarly, recently proposed solar energy conversion technologies are predicted to have very high efficiencies if sufficiently low work function anodes can be produced.[12]

To lower the work function of a material, one typical approach is to lower the vacuum level by surface engineering, particularly by depositing a very thin layer (about one monolayer) of alkali metal, such as Cs, Li, Sr, or Ba,[13−16] that are sometimes combined with a proper amount of oxygen. Among these approaches, Cs/O coated materials typically have the lowest work function between 1.1 and 1.4 eV.[17−19] The underlying mechanism for the work function reduction through the application of a thin layer of Cs/O has been extensively studied in the 1960s and 1970s, primarily driven by the development of negative electron affinity (NEA) photocathodes.[17,20−22]

Another approach to lowering the work function is to raise the material's Fermi level. In contrast to conventional three-dimensional materials, whose Fermi-level is normally "pinned" at the surface due to surface defects and traps,[23] the Fermi level of graphene (a two-dimensional material) can be effectively controlled by doping due to a lack of dangling bonds and surface states. By voltage biasing graphene relative to a gate, compensating charges build up in the graphene. This excess population of carriers shifts the Fermi level relative to its equilibrium value, thereby directly changing the graphene work

Received: May 15, 2015
Revised: September 22, 2015
Published: September 24, 2015

DOI: 10.1021/acs.nanolett.5b01916
Nano Lett. 2015, 15, 6475−6480

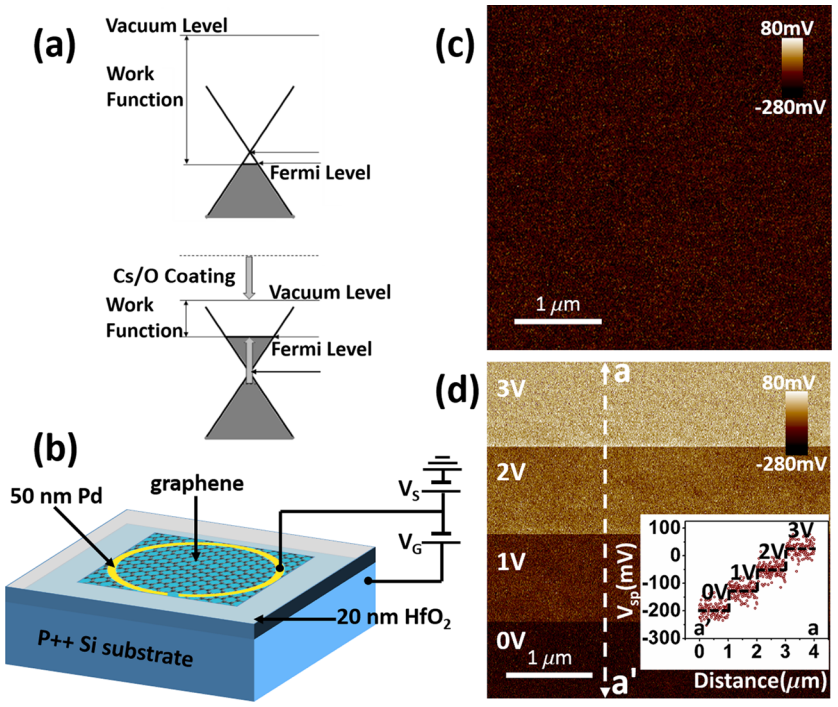

Figure 1. (a) Schematic sketch of the graphene band diagram. Negatively biasing graphene relative to the substrate raises the Fermi level, while low work function coatings like Cs/O lower the vacuum level by forming strong surface dipoles. (b) Schematic sketch of the back-gated device structure. During SKPFM measurement, graphene is grounded with V_S = 0 V, while during the photoemission experiment, V_S = −15 V to help the energy analyzer collect emitted electrons. (c) SKPFM scanning image of surface potential with V_G = 0 V. The measured surface potential is the work function difference between the SKPFM tip and graphene. (d) SKPFM scanning image of the same area as c. V_G was increased by 1 V after each quarter of the area is scanned. The inset figure shows the profile of the surface potential V_{sp} along the a′−a dashed line.

function, a process known as electrostatic gating. Previous studies on electrostatic gating of graphene show around 0.3 eV work function change.[24,25] Other doping approaches, including chemical doping and contact doping, can yield a larger work function change, on the order of 0.5−1 eV[26−30] but are less convenient and the doping level is not dynamically adjustable as it is for electrostatic gating. In addition, optical doping by photoexcited carriers has been shown to adjust the Fermi level, but the shift is only about 50 meV.[31] As the work function of undoped graphene is in a similar range as graphite, ∼4.6 eV,[32] neither of these three methods are able to yield an ultralow work function.

In this study, we combine surface engineering with electrostatic gating approaches to simultaneously lower the vacuum level and raise the Fermi level (Figure 1a), thus maximizing the work function reduction of graphene. We first use scanning Kelvin probe force microscope (SKPFM) to measure the work function of back-gated graphene with electrostatic gating alone. As SKPFM can scan rapidly and is very sensitive to the local surface potential change[33,34] it is ideal for measuring dynamic changes in the work function. Due to electrostatic gating, the carrier concentration, and thereby the Fermi level, are controlled by the back-gated voltage V_G (Figure 1b). As the Fermi level shifts, the relative potential between graphene and the metallic tip of the SKPFM change accordingly, which is also reflected by a change of conductivity. Based on a graphene transport model,[35−37] we also measure the Fermi level shift through the V_G-controlled drain current I_D. Finally, we determine experimentally the optimal amount of Cs and O_2 on our back-gated graphene device in an ultrahigh vacuum (UHV) environment and measure its work function using photoemission. We find that this low work function coating dramatically lowered the vacuum level. By combining this low work function coating with electrostatic gating, we are able to reduce the graphene work function to nearly 1 eV.

The back-gated device structure is shown schematically in Figure 1b, where graphene is electrically isolated from the conductive silicon substrate by a 20 nm thick HfO_2 dielectric layer. The silicon substrate is boron-doped (p++) with N_A = 2.69 × 10^{19} cm^{-3} and functions as a back-gate. Graphene is prepared by chemical vapor deposition (CVD) grown on copper foil (from BGTMaterials). It is then cut into 5 × 5 mm^2 pieces and transferred onto the HfO_2 dielectric layer using a standard process.[38] (For conductivity measurements, it is cut into 1 × 5 mm^2.) The surface topography of graphene is characterized by atomic force microscopy (AFM), which shows good single layer uniformity (see Figure S1 in the Supporting Information). The HfO_2 layer is deposited on the silicon substrate using atomic layer deposition (ALD) (see Supporting Information). After the graphene transferring, 50 nm thick Pd contact electrodes are thermally evaporated through a shadow mask. The SKPFM tool is first used for work function measurement with a platinum−iridium coated tip in room ambient, without a Cs/O coating layer on the graphene. The SKPFM image is recorded in a multi lock-in, single pass tapping mode. During the measurement, the tip is constantly tapping the sample surface with the resonant frequency of the cantilever, which is around 60 kHz, with the amplitude of typically 25 nm. The AFM signal is obtained simultaneously. In our UHV chamber of about 5 × 10^{-10} Torr, a hemispherical capacitive electron energy analyzer is used to measure the work function from photoemission using a 100 eV synchrotron soft X-ray both before and after Cs/O layer deposition.

DOI: 10.1021/acs.nanolett.5b01916
Nano Lett. 2015, 15, 6475−6480

We start our investigation by comparing the graphene surface potential V_{sp} with and without V_G, while keeping the graphene and SKPFM tip grounded. When V_G = 0 V, the surface potential is uniformly distributed at about −200 mV, relative to the SKPFM tip (Figure 1c). This indicates good uniformity and cleanness of the graphene film, as multilayer graphene[39,40] and surface contamination (see Figure S2 in Supporting Information) can lead to varying surface potentials. Keeping everything else the same, we then increase V_G by 1 V from 0 V after each quarter of the same area is scanned. As shown in Figure 1d, after each step increase in V_G, the surface potential increases accordingly, indicating that its Fermi level shifts up, due to electrostatically doped electrons. The surface potential profile along the white dashed line is plotted as the inset in Figure 1d, which shows a change of 231 meV between V_G = 0 V and V_G = 3 V.

After scanning the surface potential, we keep the SKPFM tip at a fixed position and sweep V_G in order to quantify its control of the graphene work function. For each measured surface potential, the related work function can be found from $\Phi = \Phi_{tip} - qV_{sp}$, where Φ_{tip} is calibrated to be Φ_{tip} = 4.72 ± 0.02 eV using highly oriented pyrolytic graphite (HOPG) as reference (see Figure S3 in Supporting Information). Figure 2 shows the

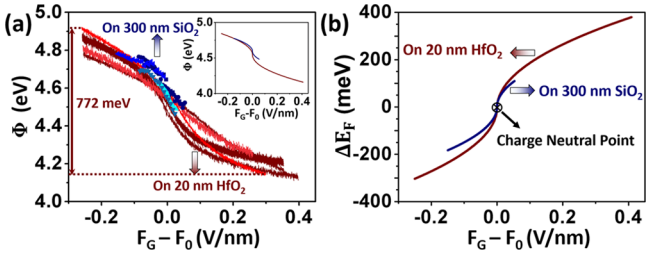

Figure 2. (a) Local work function measured by SKPFM as a function of $F_G - F_0$ for five samples (reddish), compared to literature measurements using 300 nm SiO_2 as dielectric layer (blueish).[24] Notably, the largest work function shift observed from one of our samples is 772 meV. The inset shows the least-squares fittings to both data sets by $\Phi = \text{sign}(F_G - F_0)\cdot a(|F_G - F_0|)^{1/2} + \Phi_i$, where $a = \hbar v_F(\pi\varepsilon_{ox}/e)^{1/2}$, from which we get F_0 = 0.05 ± 0.01 V/nm. (b) Calculated Fermi level shift ($\Delta E_F = \Phi_i - \Phi$) a function of $F_G - F_0$ corresponding to the inset in a.

work function of five samples as a function of $F_G - F_0$, where F_G is the gate electric field within the HfO_2 dielectric layer, and F_0 is charge neutral electric field when Fermi level is at the Dirac point. Our result (reddish) is compared to literature measurements using 300 nm SiO_2 as dielectric layer (blueish).[24] On average, the range of field-tuned work function change of graphene on HfO_2 more than doubles what is measured on SiO_2, due to higher dielectric constant as well as higher breakdown electric field. Notably, the largest work function change observed from one of our samples is 772 meV.

As a first-order approximation using the linear energy dispersion of graphene,[41] the work function is described as

$$\Phi = \text{sign}(F_G - F_0)\hbar v_F\sqrt{\pi}\sqrt{\varepsilon_{ox}|F_G - F_0|/q} + \Phi_i$$

where Φ_i is the intrinsic work function of graphene when at the neutral charge point, v_F is the graphene Fermi velocity, ε_{ox} is the relative permittivity of the dielectric layer, and q is the elementary charge. Since substrate inversion is not observed within the range of applied substrate voltage, the p-type silicon substrate will either be accumulated, for $V_G > V_{FB}$, where V_{FB} is the flat band voltage, or depleted, for $V_G < V_{FB}$. Based on the basics of metal-oxide-semiconductors system (MOS),[42] the electric field F_G in both regions is

$$F_G = \begin{cases} (V_G - V_{FB})/t_{ox} & (V_G > V_{FB}) \\ \dfrac{qN_A\varepsilon_{Si}}{C_{ox}^2 t_{ox}}\left[\sqrt{1 + \dfrac{2C_{ox}^2(V_G - V_{FB})}{q\varepsilon_{Si}N_A}} - 1\right] & (V_G < V_{FB}) \end{cases}$$

where $C_{ox} = \varepsilon_{ox}/t_{ox}$ is the capacitance of HfO_2 with t_{ox} = 20 nm, $\varepsilon_{ox} = 10.4\varepsilon_0$ for HfO_2, $\varepsilon_{ox} = 3.9\varepsilon_0$ for SiO_2, and $\varepsilon_{Si} = 11.7\varepsilon_0$, where ε_0 is the permittivity of vacuum. The dielectric constant of our HfO_2 film is measured from a metal-oxide-semiconductor capacitor (MOSCAP) control device with 200 nm thick Al gate electrode. The flat band voltage $V_{FB} = \Phi_{Si} - \Phi$, where Φ_{Si} = 5.17 eV is the calculated work function of the silicon substrate. Note that the second term indicates that V_{FB} is a function of the graphene work function. Applying a least-squares fit using the above relationship with v_F, Φ_i and F_0 as the fitting parameters, we find $v_F = (1.20 \pm 0.03) \times 10^6$ m/s and Φ_i = 4.52 ± 0.02 eV for our HfO_2 samples. The charge-neutral electric field of our samples is found to be positive, $F_0 \approx 0.05$ V/nm, indicating that graphene is initially slightly p-type.

To confirm the work function shifts observed are due to changes in graphene Fermi level E_F, we have measured the conductivity of graphene as a function of F_G, which can be directly mapped to E_F based on the transport model.[35−37] Three-terminal transistor-structure devices are fabricated to measure the drain current I_D of graphene as a function of F_G (Figure 3a). Figure 3b plots the variation of I_D with respect to

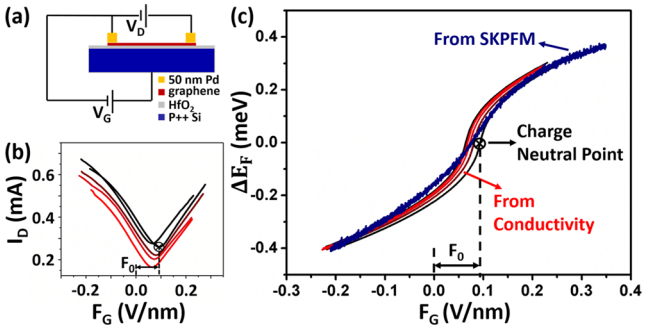

Figure 3. (a) Schematic diagram of the conductivity measurement setup. The graphene channel is 5 mm long and 1 mm wide. Drain voltage is V_D = 1 V. (b) Variation of the drain current I_D as a function of F_G. The minimum I_D corresponding to the charge neutral point on average is shifted by F_0 = 0.07 ± 0.01 V/nm, which is consistent with the SKPFM results. (c) Plot of Fermi level as a function of F_G obtained from (b) (reddish curves). All five samples show very similar Fermi level shift behaviors. The blue curve is obtained from one of the SKPFM work function curves in Figure 2a, which matches the conductivity measurement result remarkably well.

F_G for an additional five different samples from the same batch used in SKPFM measurement except the geometry of graphene and its contact. The charge-neutral electric field is averaged to be $F_0 \approx 0.07$ V/nm, which is consistent with the SKPFM results, confirming the initial p-type for graphene. The electron and hole concentrations are directly found from the measured resistance, $R_{measure} = 2R_C + R_{series} + R_{graphene}$, where R_C is the contact resistance, $R_{graphene} = (L/W)[q\mu_0(n + p)]^{-1}$ is the graphene resistance with L/W = 5 as its channel length to width ratio, n and p are the hole and electron concentrations,

DOI: 10.1021/acs.nanolett.5b01916
Nano Lett. 2015, 15, 6475−6480

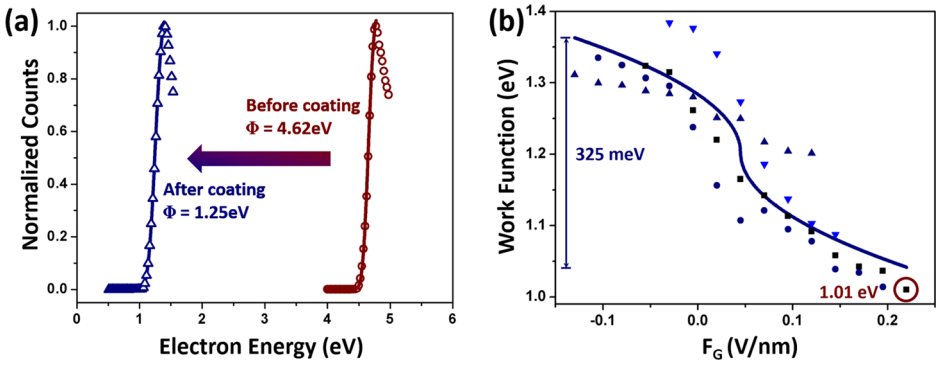

Figure 4. (a) Low kinetic energy cutoff comparison with and without Cs/O coating at F_G = 0 V/nm measured by photoemission in an UHV environment. The solid line is the complementary error function fitting by $y = a\ \mathrm{erfc}[(x - \Phi)/b] + c$ from which Φ is extracted.[44] After an optimal amount of Cs and O_2 is coated, the work function is dramatically reduced by over 3 eV (b) work function of graphene as a function of F_G for four different samples from the same batch as in SKPFM, with Cs/O coating. A constant interval of 45 s is maintained between each measurement, and the leakage current across HfO_2 is kept within 1 μA for all V_G. The charge neutral point isF_0 = 0.04 ± 0.01 V/nm. Notably, at F_G = 0.2 V/nm, the work function is as low as 1.01 ± 0.05 eV.

and R_{series} = 5 Ω is the estimated series resistance from the external test circuit. Based on the conductivity results shown in Figure 3b, the graphene Fermi level as a function of F_G is found and shown in Figure 3c as blue curves. The least-squares fitting shows $v_F = (1.57 \pm 0.03) \times 10^6$ m/s, which is slightly larger than observed in SKPFM, but in generally good agreement.

In addition to testing in room air ambient, we have measured photoemission from our graphene devices in UHV (5×10^{-10} Torr) using soft X-ray illumination. We first anneal our sample at ∼300 °C for 30 min in this vacuum in order to clean the graphene surface.[43] We then illuminate the sample with 100 eV synchrotron X-rays on a 1 × 1 mm spot, with surface potential V_S = −15 V applied to graphene (Figure 1b) to accelerate emitted electrons to the grounded energy analyzer. We extract the work function from $\Phi = K_{LEC} + \Phi_{analyzer} - qV_S$, where $\Phi_{analyzer}$ = 4.1 eV is the analyzer's work function, and K_{LEC} is the low kinetic energy cutoff obtained from photoemission spectroscopy. The electron energy with respect to the Fermi level is plotted in Figure 4a, from which the work function can be found out by fitting the curve with complementary error function[44] $y = a\ \mathrm{erfc}[(x - \Phi)/b] + c$. After annealing, the work function of graphene is Φ = 4.62 ± 0.08 eV, very close to SKPFM result.

We then investigate in situ coating graphene with Cs and O to achieve one of the lowest work function values ever reported (with structure shown in Figure 1b). The Cs/O deposition is performed following the typical photocathode activation technique[17] in our UHV chamber for maximizing the sample's quantum efficiency which is concurrently monitored with a blue laser (405 nm). The deposition details are included in Section 4 of the Supporting Information. After the deposition, the work function is dramatically lowered from 4.62 eV down to 1.25 eV. We have monitored the graphene resistance before and after the Cs/O deposition, showing only ∼15% change (see Section 6 in Supporting Information), indicating that the quality of the graphene is not significantly affected during this process. Unfortunately, since the Cs/O layer is extremely sensitive to environmental conditions, we are not able to perform either SPKFM/AFM or three-terminal conductivity measurement after the coating.

This large work function reduction is due to the strong surface dipole from the Cs/O coating, as has been found on many other substrate materials, including InP,[20] GaAs,[17,21] and $Ga_{1-x}In_xAs$,[22] with a very similar deposition technique. The estimated thickness of our Cs/O layer on graphene is 7 ± 3 Å, similar to previous studies (see Section 5 in Supporting Information), in which the chemical composition and atomic arrangement of the thin Cs/O layer have been carefully analyzed. According to these previous studies, the Cs/O layer consists of two types of dipoles, substrate-Cs^+ and $[Cs^+]$-O^{2-}-Cs^+. The first dipole is just between the substrate and one submonolayer of Cs^+, and the other dipole is made of two submonolayers of Cs^+ with O^{2-} intercalated layer between the two Cs^+ layers. Note that the square bracket indicates some structural variation of the middle submonolayer of Cs^+ depending on the substrate. With the same deposition technique, similar quantum efficiency behavior during deposition (see Figure S4 in Supporting Information), and similar measured thickness, it is reasonable to assume that the Cs/O layer on graphene is similar to what has been found on other substrates with the double-dipole structure, which sets the position of the new vacuum level.

Finally, we have tested whether the electrostatic gating and Cs/O coating could act in concert. Figure 4b displays the work function of graphene as a function of F_G with Cs/O coating (scattered symbols) for four different samples from the same batch as SKPFM. The solid blue line is the least-squares fitting performed in the same way as in the inset of Figure 2a. As shown in Figure 4b, the tunability of the graphene work function by back-gated electric field still remained with Cs/O coatings, although it is moderated, and the breakdown electric field of HfO_2 is decreased, resulting in smaller range of F_G that could be applied. The tunability is about 325 meV from F_G of −0.15 V/nm to 0.2 V/nm, compared to about 550 meV from SKPFM in the same range. This reduction of tunability could result from multiple factors. One could be the interaction between Cs/O coating and graphene. The other, which maybe more important, is that the measured area is much larger, 1 mm in diameter compared to 1 μm in SKPFM, which makes surface contamination and defects more important. Notably, at F_G = 0.2 V/nm on one of our samples, we observed the lowest work function reported so far for graphene system: 1.01 ± 0.05 eV, which is also the lowest reported to date for a conductive, nondiamond sample.

In summary, we have demonstrated that the work function can be lowered to nearly 1 eV by combining electrostatic gating

DOI: 10.1021/acs.nanolett.5b01916
Nano Lett. 2015, 15, 6475−6480

with surface engineering techniques for the graphene system studied in this work. Due to its two-dimensionality and low surface density of states, electrostatic gating can effectively control the graphene work function by changing its Fermi level. Furthermore, by coating the surface with optimal amount of Cs and O_2, the work function can be reduced even further due to the lowering of vacuum level at the surface. This combination approach demonstrated here provides a route toward ultralow work function electrodes for energy conversion and electron emission applications.

■ ASSOCIATED CONTENT

Supporting Information

The Supporting Information is available free of charge on the ACS Publications website at DOI: 10.1021/acs.nanolett.5b01916.

Description of the HfO_2 preparation, the AFM image of clean and contaminated graphene, the SKPFM image of the contaminated graphene and its surface potential response to V_G, the calibration of the work function of SKPFM probes, the details of Cs/O deposition, the thickness analysis of Cs/O layer, and the graphene resistance change before and after Cs/O deposition (PDF)

■ AUTHOR INFORMATION

Corresponding Author

*E-mail: hongyuan.yuan36@gmail.com.

Notes

The authors declare no competing financial interest.

■ ACKNOWLEDGMENTS

We thank Dr. Song Xu from Keysight Technology for his valuable technical support on SKPFM measurement. We also thank Dr. Zhi Liu for his clear and patient explanation on his previous study on the Cs/O layer. This work was supported by Global Climate & Energy Project (GCEP) at Stanford University, and by the Air Force grant FA9550-14-1-0251 (N.C.W. and E.P.).

■ REFERENCES

(1) Zhou, Y.; Fuentes-Hernandez, C.; Shim, J.; Meyer, J.; Giordano, A. J.; Li, H.; Winget, P.; Papadopoulos, T.; Cheun, H.; Kim, J.; Fenoll, M.; Dindar, A.; Haske, W.; Najafabadi, E.; Khan, T. M.; Sojoudi, H.; Barlow, S.; Graham, S.; Brédas, J.-L.; Marder, S. R.; Kahn, A.; Kippelen, B. *Science* **2012**, *336* (6079), 327−332.

(2) Chen, H.-Y.; Hou, J.; Zhang, S.; Liang, Y.; Yang, G.; Yang, Y.; Yu, L.; Wu, Y.; Li, G. *Nat. Photonics* **2009**, *3* (11), 649−653.

(3) Yan, H.; Chen, Z.; Zheng, Y.; Newman, C.; Quinn, J. R.; Dotz, F.; Kastler, M.; Facchetti, A. *Nature* **2009**, *457* (7230), 679−686.

(4) Friend, R. H.; Gymer, R. W.; Holmes, A. B.; Burroughes, J. H.; Marks, R. N.; Taliani, C.; Bradley, D. D. C.; Santos, D. A. D.; Bredas, J. L.; Logdlund, M.; Salaneck, W. R. *Nature* **1999**, *397* (6715), 121−128.

(5) Lee, J.-H.; Bargatin, I.; Vancil, B. K.; Gwinn, T. O.; Maboudian, R.; Melosh, N. A.; Howe, R. T. *J. Microelectromech. Syst.* **2014**, *23* (5), 1182−1187.

(6) Lee, J.; Bargatin, I.; Provine, J.; Clay, W.; Schwede, J.; Liu, F.; Maboudian, R.; Melosh, N.; Shen, Z.; Howe, R. *Technol. Dig. Power MEMS* **2009**, 6−9.

(7) Meir, S.; Stephanos, C.; Geballe, T. H.; Mannhart, J. *J. Renewable Sustainable Energy* **2013**, *5* (4), 043127.

(8) Wang, Y.; Su, S.; Lin, B.; Chen, J. *J. Appl. Phys.* **2013**, *114* (5), 053502.

(9) Yaghoobi, P.; Vahdani Moghaddam, M.; Nojeh, A. *AIP Adv.* **2012**, *2* (4), 042139.

(10) Lee, J. I.; Jeong, Y. H.; No, H.-C.; Hannebauer, R.; Yoo, S.-K. *Appl. Phys. Lett.* **2009**, *95* (22), 223107.

(11) Littau, K. A.; Sahasrabuddhe, K.; Barfield, D.; Yuan, H.; Shen, Z.-X.; Howe, R. T.; Melosh, N. A. *Phys. Chem. Chem. Phys.* **2013**, *15* (34), 14442−14446.

(12) Schwede, J. W.; Bargatin, I.; Riley, D. C.; Hardin, B. E.; Rosenthal, S. J.; Sun, Y.; Schmitt, F.; Pianetta, P.; Howe, R. T.; Shen, Z.-X.; Melosh, N. A. *Nat. Mater.* **2010**, *9* (9), 762−767.

(13) Psarouthakis, J. *Surf. Sci.* **1969**, *17* (2), 316−332.

(14) Chou, S. H.; Voss, J.; Vojvodic, A.; Howe, R. T.; Abild-Pedersen, F. *J. Phys. Chem. C* **2014**, *118* (21), 11303−11309.

(15) Brodie, I.; Chou, S. H.; Yuan, H. *Surf. Sci.* **2014**, *625* (0), 112−118.

(16) O'Donnell, K. M.; Martin, T. L.; Fox, N. A.; Cherns, D. *Phys. Rev. B: Condens. Matter Mater. Phys.* **2010**, *82* (11), 115303.

(17) Su, C. Y.; Spicer, W. E.; Lindau, I. *J. Appl. Phys.* **1983**, *54* (3), 1413−1422.

(18) Desplat, J. L.; Papageorgopoulos, C. A. *Surf. Sci.* **1980**, *92* (1), 97−118.

(19) Sun, Y.; Liu, Z.; Pianetta, P.; Lee, D.-I. *J. Appl. Phys.* **2007**, *102* (7), 074908.

(20) Lee, D.-I.; Sun, Y.; Liu, Z.; Sun, S.; Peterson, S.; Pianetta, P. *J. Appl. Phys.* **2007**, *102* (7), 074909.

(21) Sommer, A. H.; Whitaker, H. H.; Williams, B. F. *Appl. Phys. Lett.* **1970**, *17* (7), 273−274.

(22) Fisher, D. G.; Enstrom, R. E.; Escher, J. S.; Williams, B. F. *J. Appl. Phys.* **1972**, *43* (9), 3815−3823.

(23) Allen, F. G.; Gobeli, G. W. *Phys. Rev.* **1962**, *127* (1), 150−158.

(24) Yu, Y.-J.; Zhao, Y.; Ryu, S.; Brus, L. E.; Kim, K. S.; Kim, P. *Nano Lett.* **2009**, *9* (10), 3430−3434.

(25) Copuroglu, M.; Aydogan, P.; Polat, E. O.; Kocabas, C.; Süzer, S. *Nano Lett.* **2014**, *14* (5), 2837−2842.

(26) Shi, Y.; Kim, K. K.; Reina, A.; Hofmann, M.; Li, L.-J.; Kong, J. *ACS Nano* **2010**, *4* (5), 2689−2694.

(27) Shin, H.-J.; Choi, W. M.; Choi, D.; Han, G. H.; Yoon, S.-M.; Park, H.-K.; Kim, S.-W.; Jin, Y. W.; Lee, S. Y.; Kim, J. M.; Choi, J.-Y.; Lee, Y. H. *J. Am. Chem. Soc.* **2010**, *132* (44), 15603−15609.

(28) Giovannetti, G.; Khomyakov, P. A.; Brocks, G.; Karpan, V. M.; van den Brink, J.; Kelly, P. J. *Phys. Rev. Lett.* **2008**, *101* (2), 026803.

(29) Hwang, J. O.; Park, J. S.; Choi, D. S.; Kim, J. Y.; Lee, S. H.; Lee, K. E.; Kim, Y.-H.; Song, M. H.; Yoo, S.; Kim, S. O. *ACS Nano* **2012**, *6* (1), 159−167.

(30) Yang, S.; Zhou, P.; Chen, L.; Sun, Q.; Wang, P.; Ding, S.; Jiang, A.; Zhang, D. W. *J. Mater. Chem. C* **2014**, *2* (38), 8042−8046.

(31) Qi, J.; Zhang, H.; Ji, D.; Fan, X.; Cheng, L.; Liang, H.; Li, H.; Zeng, C.; Zhang, Z. *Adv. Mater.* **2014**, *26* (22), 3735−3740.

(32) Takahashi, T.; Tokailin, H.; Sagawa, T. *Phys. Rev. B: Condens. Matter Mater. Phys.* **1985**, *32* (12), 8317−8324.

(33) Filleter, T.; Emtsev, K. V.; Seyller, T.; Bennewitz, R. *Appl. Phys. Lett.* **2008**, *93* (13), 133117.

(34) Rosenwaks, Y.; Shikler, R.; Glatzel, T.; Sadewasser, S. *Phys. Rev. B: Condens. Matter Mater. Phys.* **2004**, *70* (8), 085320.

(35) Dorgan, V. E.; Bae, M.-H.; Pop, E. *Appl. Phys. Lett.* **2010**, *97* (8), 082112.

(36) Fang, T.; Konar, A.; Xing, H.; Jena, D. *Appl. Phys. Lett.* **2007**, *91* (9), 092109.

(37) Bae, M.-H.; Islam, S.; Dorgan, V. E.; Pop, E. *ACS Nano* **2011**, *5* (10), 7936−7944.

(38) Liang, X.; Sperling, B. A.; Calizo, I.; Cheng, G.; Hacker, C. A.; Zhang, Q.; Obeng, Y.; Yan, K.; Peng, H.; Li, Q.; Zhu, X.; Yuan, H.; Hight Walker, A. R.; Liu, Z.; Peng, L.-m.; Richter, C. A. *ACS Nano* **2011**, *5* (11), 9144−9153.

(39) Hibino, H.; Kageshima, H.; Kotsugi, M.; Maeda, F.; Guo, F. Z.; Watanabe, Y. *Phys. Rev. B: Condens. Matter Mater. Phys.* **2009**, *79* (12), 125437.

(40) Datta, S. S.; Strachan, D. R.; Mele, E. J.; Johnson, A. T. C. *Nano Lett.* **2009**, *9* (1), 7−11.

DOI: 10.1021/acs.nanolett.5b01916
Nano Lett. 2015, 15, 6475−6480

(41) Avouris, P.; Chen, Z.; Perebeinos, V. *Nat. Nanotechnol.* **2007**, *2* (10), 605−615.
(42) Howe, R. T.; Sodini, C. G. *Microelectronics: An Integrated Approach*; Prentice Hall: Upper Saddle River, 1996.
(43) Siokou, A.; Ravani, F.; Karakalos, S.; Frank, O.; Kalbac, M.; Galiotis, C. *Appl. Surf. Sci.* **2011**, *257* (23), 9785−9790.
(44) Mathieu, C.; Barrett, N.; Rault, J.; Mi, Y. Y.; Zhang, B.; de Heer, W. A.; Berger, C.; Conrad, E. H.; Renault, O. *Phys. Rev. B: Condens. Matter Mater. Phys.* **2011**, *83* (23), 235436.

DOI: 10.1021/acs.nanolett.5b01916
Nano Lett. 2015, 15, 6475−6480